Some aspects of the deep abyssal overflow between the middle and southern basins of the Caspian Sea

Javad Babagoli Matikolaei[1], Abbasali Aliakbari Bidokhti[2], and Maryam Shiea[3]

[1]Graduate in Physical Oceanography, Institute of Geophysics, University of Tehran, Tehran, Iran.
[2]Institute of Geophysics, University of Tehran, Tehran, Iran.
[3]Faculty of Marine Science and Technology, Science and Research Branch, Islamic Azad University, Tehran, Iran.

Corresponding Author: Abbasali Aliakbari Bidokhti (bidokhti@ut.ac.ir)

Abstract. The present study investigates the deep gravity current between the middle and southern Caspian Sea basins, caused by the density difference of deep waters. Oceanographic data, numerical model, and dynamic models are used to consider the structure of this Caspian Sea abyssal overflow. The CTD data are obtained from UNESCO, and the three-dimensional ocean model COHERENS results are used to study the abyssal currents in the southern basin of the Caspian Sea. The deep overflow is driven by the density difference mainly due to the temperature difference between the middle and southern basins, especially in winter. Due to cold weather in the northern basin, water sinks in high latitudes and after filling the middle basin it overflows into the southern basin. As the current passes through the Absheron Strait (or sill), we use the analytic model of Falcini and Salusti (2015) for the overflow gravity current to estimate the changes of vorticity and potential vorticity of the flow over the Absheron sill; the effects of entrainment and friction are also considered. Because of the importance of the overflow in deep water ventilation, a simple dynamical model of the boundary currents based on the shape of the Absheron Strait is used to estimate typical mass transport and flushing time which is found to be about 15 to 20 years for the southern basin of the Caspian Sea. This time scale is important for the Caspian Sea ecosystem and the impacts of pollution due to oil exploration. Apart from this, by reviewing the drilled oil and gas wells in the Caspian Sea, the results show that the deep overflow moves over some of these wells. Thus, the deep flow can be an important factor of oil pollution in the deeper part of the southern Caspian Sea.

Keywords: Overflow, dynamical model, trapped baroclinic bottom current, Caspian Sea abyssal flow.

1. Introduction

Baroclinic currents play an important role in the ocean and sea circulations, especially in deep waters of the ocean. Because these currents are important in deep water ventilations of the oceans, they have an integral role in thermohaline circulation. A driving mechanism for the circulation is cooling of surface waters at high latitudes and consequent formations of deep waters by sinking the cooled salty water masses (Fogelqvist et al., 2003).

Cooling in polar seas (Dickson et al., 1990) and evaporation in marginal seas (Baringer and Price, 1997) form dense waters that sink to form deep water masses. For example, dense water from the deep convective regions of the North Atlantic produces a signature of the thermohaline overturning circulation that can be seen as far away as the Pacific and Indian oceans (Girton et al., 2003). In the global sense, bottom-trapped currents play an integral role in thermohaline circulation and are a vehicle for the transport of heat, salt, oxygen, and nutrients over great distances and depths. Mixing and exchange processes between along-slope currents at the continental shelves and deep ocean water can also affect the thermohaline circulations. Huthnance (1995) has reviewed the processes involved in such near-shelf circulations. He has pointed out such flows around the world that may lead to the formation of mesoscale eddies as they become unstable while moving along the sloped boundary. The ability of abyssal flows to transport and deposit sediments is also of geological interest (Smith, 1975).

As thermohaline circulation causes ventilation of deep ocean water, it is important not only in open seas and ocean but also in semi-closed and closed basins ventilations, e.g. the Caspian Sea. Study of thermohaline dynamics and circulation has also been of interest to other scientists such as climate researchers. The dynamics of such dense currents on slopes have been modeled in the past both theoretically and experimentally starting with Ellison and Turner (1959) and Britter and Linden (1980), and a review on gravity currents can be found in Griffiths (1986).

The Caspian Sea, the world's largest inland enclosed water body, consists of three basins namely northern(shallow, mean depth of about 10 m and covering 80000 km^2), the middle (rather deep, with mean depth of about 200 m, maximum depth 788 m and covering 138000 km^2) and the southern (deep, with a mean depth of 350 m, maximum depth 1025 m and covering 164840 km^2) and is located between 36.5° N and 47.2° N, and 46.5° E and 54.1° E (Aubrey et al., 1994; Aubrey, 1994). The depth varies greatly over this sea (Ismailova, 2004, Figure 1). The northern basin, after a sudden depth transition at the shelf edge, reaches the middle one. The middle and southern basins are divided by the Absheron sill or Strait (with a maximum depth of 180m). The western slopes of the two deeper basins are fairly steep compared to the eastern slope (Gunduz and Özsoy, 2014). Peeters et al (2000) have also estimated the ages of waters of the Caspian Sea basins while considering the exchange between the middle and southern basins, based on chemical tracers, and found typical ages of about 20 to 25 years depending on the exchange rates. The exchange rate between the middle and southern basins seems to vary year by year and is dominated by atmospheric forcing (and sea level change).

The Caspian Sea is enclosed with weak tides and its circulation is mainly due to wind and buoyancy, although some wave-driven flows also occur in coastal regions (Bondarenko, 1993; Ghaffari and Chegini, 2010; Ghaffari et al., 2013; Ibrayev et al., 2010; Terziev et al., 1992). The seasonal circulation based on a coupled sea hydrodynamics, air-sea interaction and sea ice

thermodynamics model of the Caspian Sea was investigated by Ibrayev et al. (2010) and Gunduz and Özsoy (2014). The effect of freshwater inflow to the Caspian Sea on seasonal variations of salinity and surface circulation (or flow) pattern of the Caspian Sea has also been studied using HYCOM model (Kara et al, 2010). These studies indicate that in north-eastern parts of the middle basin of this sea there are signs of sinking water in cold season. Such deep convection can be a part of the thermocline circulations, affected by the side walls topography of the middle and southern basins. These deep topographically influenced rotating flows can constitute parts of the abyssal circulation of the Caspian Sea.

The main aim of the present work is to study the deep abyssal overflow in the Caspian Sea that has only been touched on in the previous studies. To fulfill this, we used observational data and numerical simulations to show that the overflow can exist over the Absheron sill. Firstly, we used observational data to understand the feasibility of the deep flow in this basin; however, the resolution of observation data is very low to cover all the purposes of the paper. Hence, the use of a numerical model can help us understand better the Absheron sill deep overflow. This paper is divided into three main parts based on the goals of the paper. Section two focuses on the existence of the deep overflow in the Caspian Sea using some observations and numerical simulations, as there has been only a little research on this deep flow in the Caspian Sea (Peeters et al, 2000). In the course of this section, the accuracy of the model simulations is considered by comparing the model results with some observational data. Section 3 concentrates on the dynamics of the outflow when moving through the Absheron Strait into the southern basin. Although there are many aspects of the dynamics of the flow, the vorticity and potential vorticity will be considered in this section. In section 4, the importance of the abyssal overflow will be indicated and the volume of this flow and hence the flushing time of the southern Caspian Sea basin will be calculated using a simple model for the overflow over the Absheron sill.

2 Data used and method of the research

2.1 Observational data

The data used in this study were taken mainly by the International Atomic Energy Agency (IAEA), in Septembers of 1995 and 1996 (Peeters et al (2000). This data are collected at 42 stations using an exploration ship, namely Hajef. The 1995 data are for 13 stations, while the 1996 data are for 29 stations (Figure 1). At first, temperature, salinity, and density diagrams are plotted for all stations. Both data sets indicate the differences between densities of deep waters of the middle and southern basins. For example, Fig. 2a shows the density differences between a and b (Fig. 1b) as about 0.5 kg/m^3. For better understanding, the *T-S* diagram is plotted to investigate the contribution of temperature and salinity in this density difference. Based on the *T-S* diagram, the water in the middle basin is both cooler and saltier than that of the southern basin, particularly in the deeper parts. Hence, the denser deeper water of the middle basin with respect of that of southern basin can lead to deep abyssal overflow between the two basins over the sill of the Absheron Strait separating middle and southern basins. The temperature, salinity and density transect across the Absheron Strait, as shown in figures 3a, b also show the evidence of the deep abyssal overflow moving from the middle to the southern basin. As the sloped isopycnals are similar to those of isotherms, it seems that the buoyancy that drives the flow is mainly due to the temperature difference. However, unfortunately, the

horizontal resolution of the measured data is not good enough to show detailed patterns of temperature, salinity, and density of the overflow (see below).

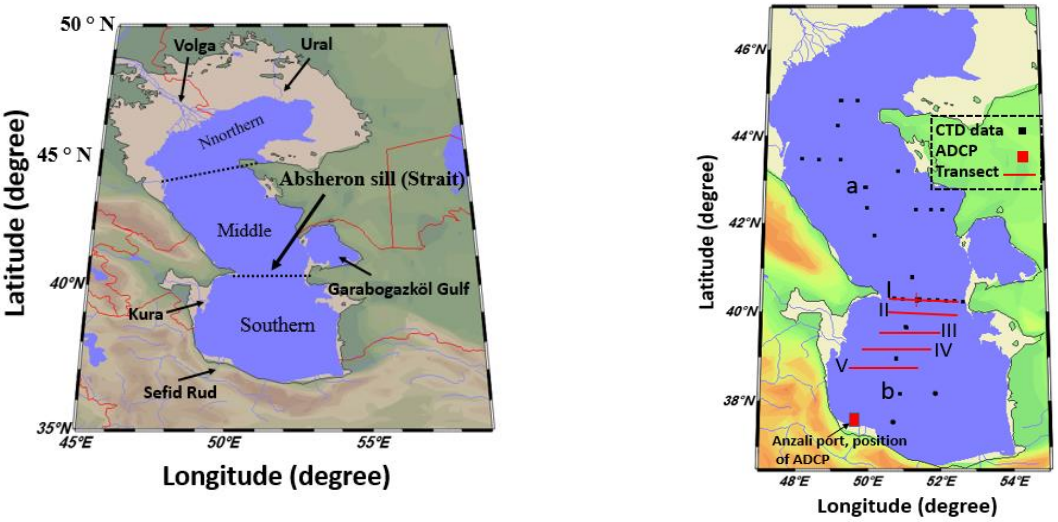

(a) **(b)**

Fig 1:(a) Schematic diagram of the Caspian Sea with the locations of the most important rivers namely the Volga, Ural and Kura and SefidRud; Garabogazköl Gulf and Absheron Strait are also shown on the map;(b) locations of CTD and ADCP measurements, the geographic position of the shown transects (see below). The CTD casts are for 42 stations for Septembers of 1995 and 1996.CTD stations, a and b are emphasized because in Fig. 2a,b, physical properties of the waters for these stations are presented. ADCP data is recorded from November 2004 to the end of January 2005 to validate the numerical simulations.

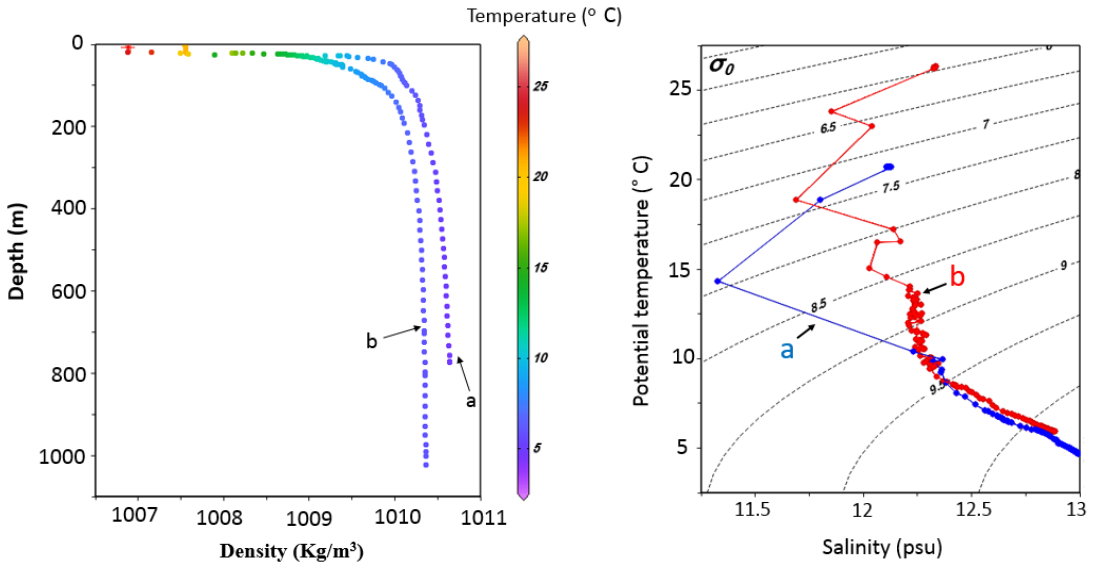

(a) **(b)**

Fig. 2: (a) Comparison of density between stations a and b (middle and southern basins, see Fig.1b) indicating the difference in density (~ 0.5 kg /m^3) between two basins. (b) *T-S* diagram for a and b to show differences in temperature and salinity,

particularly in deep water. To plot this diagram, the potential temperature and potential density anomaly (σ_0) are calculated from CTD data. The *T-S* diagram confirms the differences in density in deep water for σ_0>10 kg /m^3.

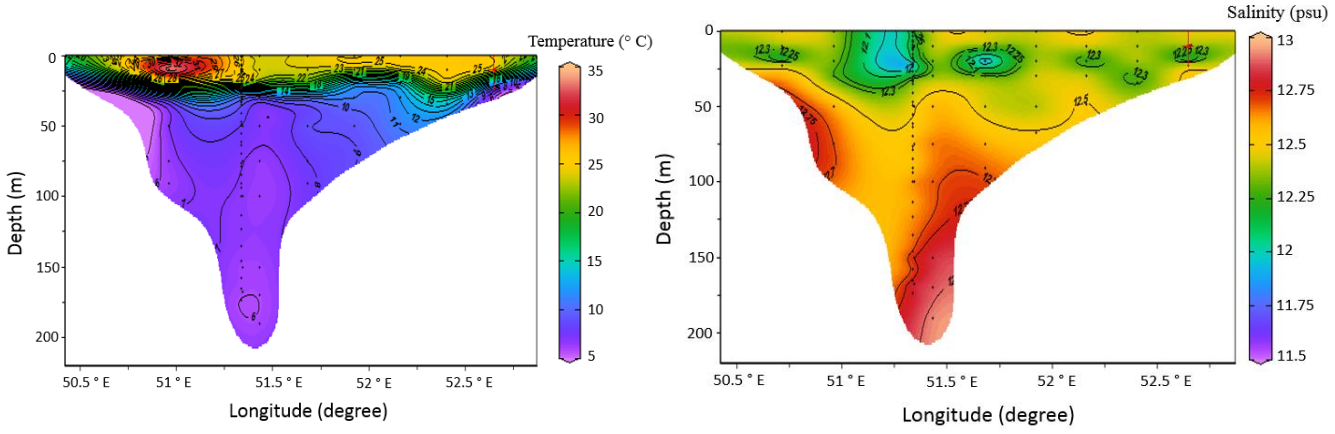

Fig. 3: Cross sections of temperature and salinity across the Strait at transect I (across the Absheron Strait over the sill) in September from observational data; dots show the locations of measurements.

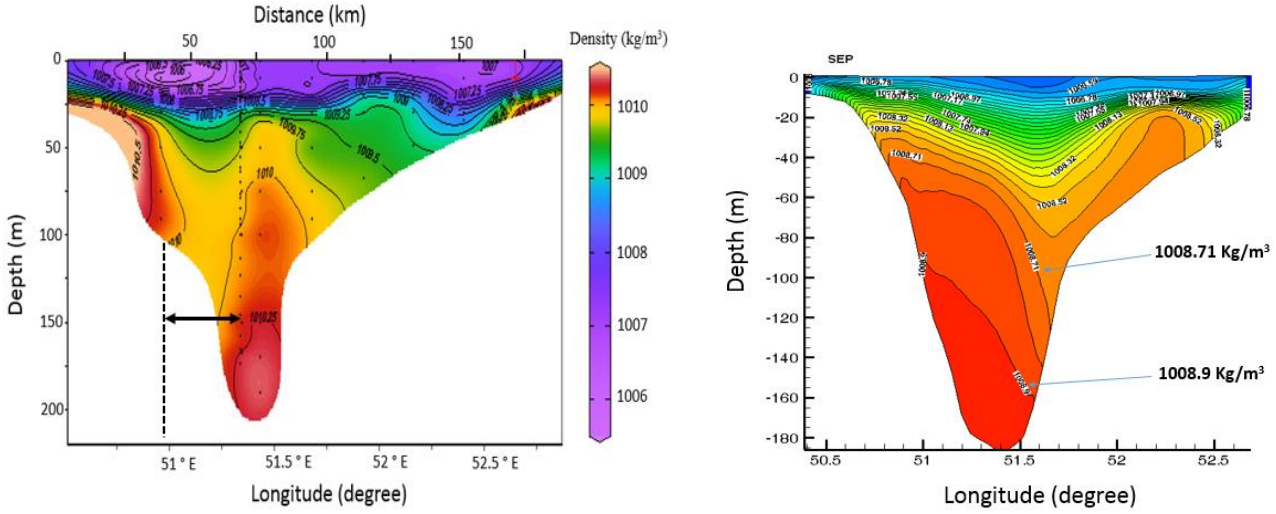

Fig.4: Comparison between density fields across the Strait in transect I, in September, from observational data (a) and numerical model (b). For observational data dots show the locations of measurements. For a better understanding of the spacing of CTD stations, distance is plotted in kilometers on the top of Fig. 4a. The cross sections are about the same but the differences between the two transects near the bottom, particularly in the west of the Strait is mainly due to the low resolution of observational data (4a). Numerical transect clearly shows the boundary trapped overflow for which two isopycnals near the bottom is highlighted (4b).

The horizontal resolution of observational data is very coarse for showing the overflow. For example, Fig 4a indicates that the width of the Strait is about 200 km and we have just 9 CTD stations. It means that the average distance between two stations is 23 km, however, unfortunately in the most important area of the Strait (western) the distance between two stations is 30-35 km. As a result, we have some problems in showing the structure of the flow. More fine-resolution data and data for different months are required to compare the cross sections of the flow for different months. Hence, due to lack of good measurements around the Strait between the two main basins of the Caspian Sea, we are compelled to use numerical simulations for the study of deep overflow at the Absheron sill, including its seasonal variability. This also includes some general aspects of the circulations in the Caspian Sea.

2.2 Some general features of the COHERENS numerical model, and its boundary and initial conditions

For the simulations, the numerical model COHERENS (Coupled Hydrodynamical Ecological model for Regional Shelf seas; Luyten et al., 1999) has been used. COHERENS uses a vertical sigma coordinate and the hydrostatic incompressible version of the Navier-Stokes equations with Boussinesq approximation and equations of temperature and salinity. The model uses an Arakawa C-grid (Arakawa and Suarez, 1983) and equations are solved numerically using the mode-splitting technique. The grid size in horizontal is 0.046 × 0.046 degrees, typically 5 km, and 30 sigma layers, labeled k (the bottom layer is 1 and the surface one is 30). The coastlines and bathymetry data with 0.5′ ×0.5′ (30 seconds) resolution are acquired from GEBCO, although interpolated and smoothed slightly.

The model was initialized for winter (January) using monthly mean temperature and salinity climatology, obtained from Kara et al (2010); and it was forced by six hourly wind, acquired from ECMWF (Mazaheri et al., 2013), and air pressure and temperature with 0.5˚×0.5˚resolution acquired from ECMWF (ERA-Interim) reanalysis. Precipitation rate, cloud cover and relative humidity (2.5˚×2.5˚) were derived from NCEP/NCAR reanalysis data. The river inflows (from the Global Run off Data Centre) were also included. The time steps of barotropic and baroclinic modes are 15 s and 150 s respectively. The total simulation time is five years (from 2000 to 2004 inclusive) with six-hour varying meteorological forcing and then the results of the last year are shown. The results of the numerical model are validated by ADCP data of the estuary between the Sefidrud River and Anzali port (figure 1, 5). These data are collected by the National Institute of Oceanography and Atmospheric Sciences, from November 2004 to the end of January 2005 (Shiea et al., 2016). This data was recorded by RCM9 current meter (at the ADCP station) at 3 depths on a mooring, near the surface, 50 m, and 200 m. The lack of observation data is the main obstacle to check the accuracy of the model results thoroughly. It would be more useful to have data on the Absheron sill for the model validation. However, using ADCP data near the Iranian coast was our only available data for model validation. For this reason, the model simulations are for five years and the results of the last year of simulations are validated with ADCP data for some months.

The simulation results of mean and long period variations of surface velocity components are rather consistent with observations. This similarity is related to the timing of flow variations rather the velocity magnitudes. The difference in velocity between observation and model simulations comes from some of the assumptions and the resolution used in the model as can

be expected. The distance between two adjacent grid points in the model is about 5 km and the ADCP data are for a point in between the two adjacent grid points, so interpolation is used to compare the model results with data at the location of observations.

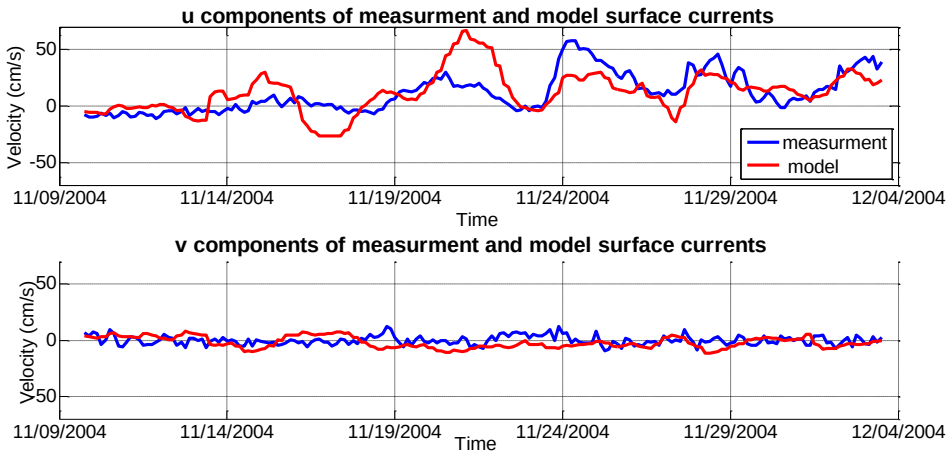

Fig. 5: Comparison between numerical model results of surface current components and observation near the Sefidrood River and Anzali port (Shiea et al., 2016).

The observational data is indicative of the existence of a deep overflow over the Absheron sill (Fig.4a). The numerical simulations also show that a deep overflow clearly exists over the sill (Fig. 4b, 6 and 14), which we examine here with more details. Typical numerical results of the deep overflow between the middle and southern basins of the Caspian Sea (the flow in the northern basin is not shown as it is too shallow) for May and December of 2004, after four years of warm-up of the model, are shown in figures6,7,8, and 14. The deep narrow flow in the middle basin and the overflow over the Absheron sill and in the northwestern boundary of the southern basin are clearly observed.

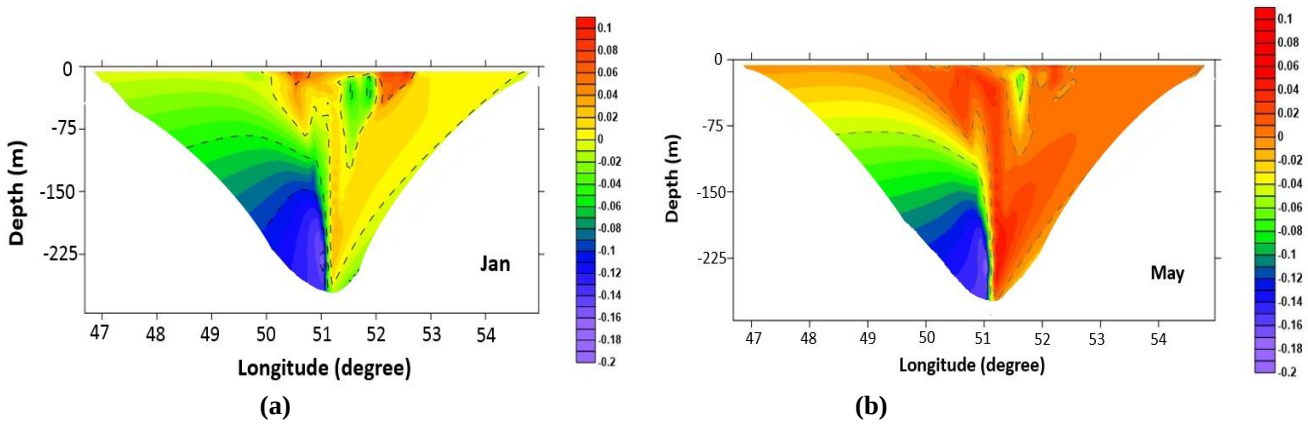

Figure 6: Cross-Section of the mean velocity (m/s) in transect I, obtained from model simulations, (a) for January and (b) May. This deep flow is southwards.

2.3 Comparison of numerical simulations with observations

The main reason for the deep flow existence in the Caspian Sea seems to be the temperature differences between the northern and southern basins. The Sea surface temperature (SST) in the northern basin ranges from below zero under frozen ice in winter to 25–26 °C in summer, while more moderate variability occurs in the southern basin changing from 7–10 °C in winter to 25°–29 °C in summer (Ibrayev et al., 2010). It shows that the water in the northern basin cools in the cold seasons so that it freezes. On the other hand, the Caspian Sea has low salinity water and in deeper parts, salinity varies little with depth (12.80–13.08 PSU), so that the density stratification largely depends on temperature variation (Terziev et al., 1992). As the northern shallow waters of the Caspian Sea are subjected to high evaporation in summer, in the following cold seasons these waters become dense and start to sink, mainly in the northeastern side of this sea (Gunduz and Özsoy, 2014). Based on the present work, the flow due to its high density enters the deep part of the middle Caspian and starts to fill the middle Caspian Sea basin. After filling the middle Caspian basin, it appears as an overflow entering into the southern basin through the Absheron Strait (Fig. 9a), similar to the that of the Denmark Strait (DS) sill (Girton et al., 2003), but the Absheron sill overflow is much smaller than that of the DS.

In order to compare the numerical simulations with observational data, some vertical distributions of temperature and density are presented (Figs.4, 8). Figure 4 indicates that the numerical model simulates the density lower than the real value in the Strait. This difference is about 0.5-1 kg/m^3 from the surface to the bottom with more difference in the deep parts. However, we can observe the similarity in the shape of the isopycnal lines between the numerical model and observations, particularly in the eastern part of the Strait. These differences are related to our assumptions and simplifications in the numerical model. We do not consider the Garabogazköl Gulf which can be an important factor for producing higher salinity water in the middle Caspian Sea basin due to high evaporation in this area (see Fig 1a). The waterway connecting the Garabogazköl Gulf to the Caspian Sea is open for some years or closed for the other years based on the fluctuation of sea surface level in the Caspian Sea. However, accurate information about the connection is not accessible for whether to include the Garabogazköl Gulf higher-salinity source in the numerical model simulations. As a result, this factor can be important in underestimation of density by the numerical model. Apart from this, the comparison of temperature between the results of the numerical and observational data indicates that the numerical model shows a higher temperature than that of observation data at the same depth (Fig.7a,b). For example, if we consider the isothermal line for the potential temperature of 6 degrees Celsius (see Fig. 7a), it is at a depth of 200-300 in the middle basin in the numerical simulations, while this isotherm is at about 200-250 m in observational data. As a result, the numerical model calculates the density less than its actual value. Based on what was mentioned, two factors contribute to the formation of deep flow between the middle and southern Caspian Sea basins. We generally conclude that the temperature factor in the formation of this deep flow is more important because the isopycnals are very similar to isotherms over the Strait (see 3a,b and 4a). Some other works also confirm the importance of temperature in the structure of circulation of water in the Caspian Sea (e.g. Terziev et al., 1992 and Ibrayev et al., 2010).

Typical Rossby number of the overflow is about $Ro = \frac{U}{fW} = 0.2/(10^{-4} \times 20 \times 10^{3}) \sim 0.1$ (here U is the typical speed of the overflow, W is its width and f if the Coriolis parameter), which justifies a geostrophic assumption for the deep overflow entering the southern basin.

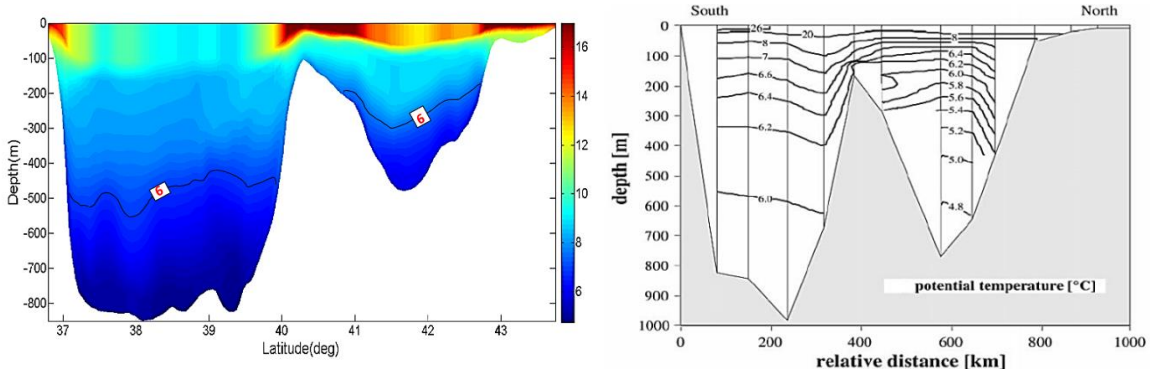

(a) **(b)**

Figure 7: Comparison between the north-south cross-sections of mean temperature obtained from model simulation (a), and Peeters et al. (2000) measurements (b) during September. The 6 °C isotherm is marked for easier comparison.

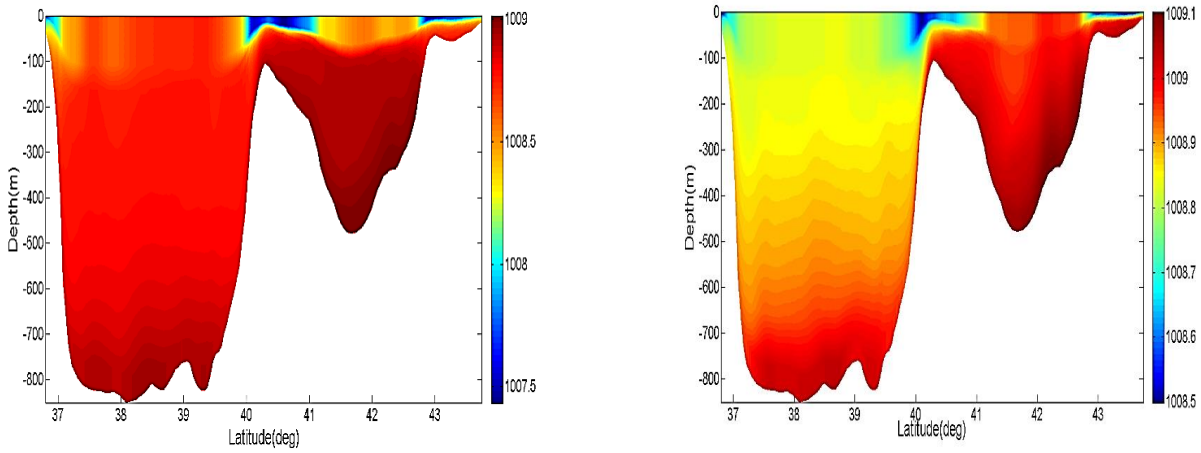

(a) **(b)**

Figure 8: Cross-Sections (N-S) of the mean density obtained from model simulation during September (a) and May (b).

Based on the numerical model, the main physical properties of water vary in different seasons. Some of the variable features of the deep overflow are shown in table 1. λ is the flow angle from the zonal east-west direction (see Fig. 9 a). Varying initial conditions for deep flow can also lead to different deep overflow behaviors in the southern basin.

Table 1: Boundary current parameters and variables obtained from the numerical simulations on the sill based on transect I (see text).

	g' (m/s^2)	v_p(m/s)	u_p(m/s)	λ(deg)
NOV	0.00222	-0.12	-0.044	107
JAN	0.00239	-0.133	-0.047	109
MAY	0.00251	-0.147	-0.031	101
SEP	0.00241	-0.19	-0.078	112

What stands out from table1 is that the main features of deep flow are different in each season. These differences show that the deep flow velocity and reduced gravity, g', fluctuate during the year, 0.127-0.2 m/s (magnitude of the velocity components) and 0.00221-0.00251m/s^2 (reduced gravity) respectively. As a result, λ is changeable between 101 and 112 degree. It is predicted that the flow may show varying behavior when moving over the Absheron sill and then into the southern basin. Here, we focus on how much water sinks with different initial conditions over the strait. To show this, some transects are plotted and are shown in Fig.10. These transects are I and II (see Fig. 1b) to evaluate how much the water sink after moving 20 km into the southern basin. The isopycnal 1008.9 *kg/m^3*is considered for all months as a reference one for the main deep flow boundary. First and most importantly, it should be close to the bottom. In addition to this, it should be better to opt for one isopycnal that is clear for all months for better comparisons. We then use one method for the flow volume flux calculation for all months. Although we could choose 1008.95 *kg/m^3* for May and September because it is closer to the bottom, it was impossible for November due to the fact that the maximum isopycnal is 1008.9 kg/m^3. Thus, we chose the 1008.9 *kg/m^3* isopycnal to estimate the flow in all transects and for all months.

Transects I and II are used due to the fact that there is only a short distance between them and because the entrainment and friction effects are less on the overflow as compared with some transects such as IV.

In this section, we investigate the effects of the different initial conditions on the deep flow. Based on the results of Fig.10, similar isopycnals are located at depths 105 m for January and 125 m for September. These depths are the mean of the maximum and minimum depths of the reference isopycnal.

The results also indicate that the deep flow in summer is confined closer to the bottom than in winter. In general, the formation mechanism of water mass can be very complex. This difficulty is related to the formation time of this water mass and how long it takes to reach the Strait. To clarify this, in the previous section we mentioned that the dense flow fills the middle basin and then overflow into the southern basin (Fig.9a). For this reason, it is tried to estimate the filling time in section four with some simplified assumptions. Peeters et al (2000) estimated the filling (or flushing) time as about 20-25 years. However, the density of water entering the southern basin is not the same for all seasons as the water sinking processes due to evaporation

and subsequent cooling in the northern basin occur mainly in winter. Nevertheless, it would be possible to track the sinking water in the strait if the numerical model simulations were at least for 20 years. The present numerical model runs are for five years only due to computing limitations. With longer simulation time it is likely that time scales of variability of the dense flow over the strait could be better investigated. It would be possible to see in which years the outflow is stronger or weaker (due to stronger or weaker atmospheric forcing) and also this could lead to the calculation of the filling time range of the basins.

Despite the fact that our simulation time was shorter (5 years) than the filling time of the middle basin which is 20 years (Peeters, et al, 2000), the simulation results for the fifth year clearly show the overflow but with some variability. This is due to fact that the initial conditions of the present numerical model are taken from the outputs of the HYCOM model simulations which were carried out by Kara et al. (2010), that has reached a more or less steady density field, close to that of the observations, after a long time (about 20 years). Previous numerical simulations did not show any significant deep flow, as such simulation times were often not enough for the whole basins to reach a quasi-steady state, as the main aims of such works only concerned the near-surface circulation processes in the Caspian Sea.

Comparison of transects I and II shows that the water sinks to depths of about 200 and 80 meters in September and January respectively, as the overflow enters the southern basin. This occurs when the water moves nearly 23 km (the distance between I and II). One of the most important reasons for this sinking depth variation can be the difference in reduced gravity that varies with season.

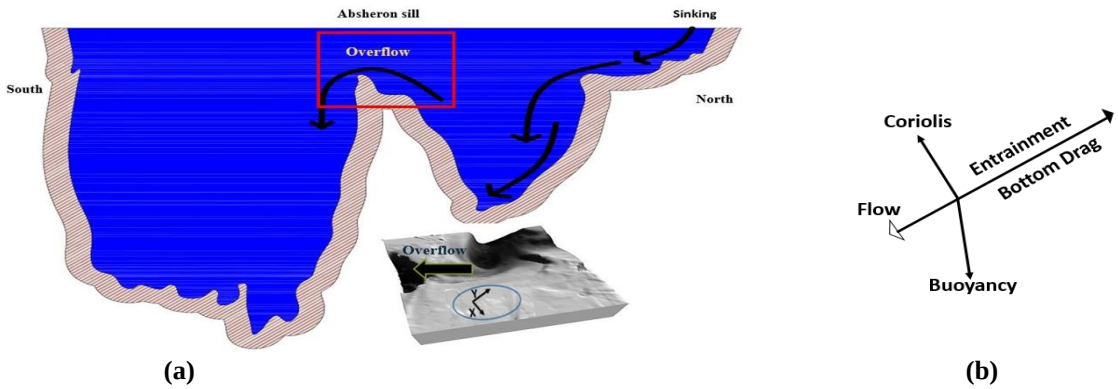

Figure 9: (a) A schematic diagram of the sinking flow in the middle basin and the overflow current over Absheron sill (top), and topography around the sill in the middle of the Caspian Sea with the chosen coordinates (bottom).(b)The balance of forces on the overflow and flow coordinates are also shown.

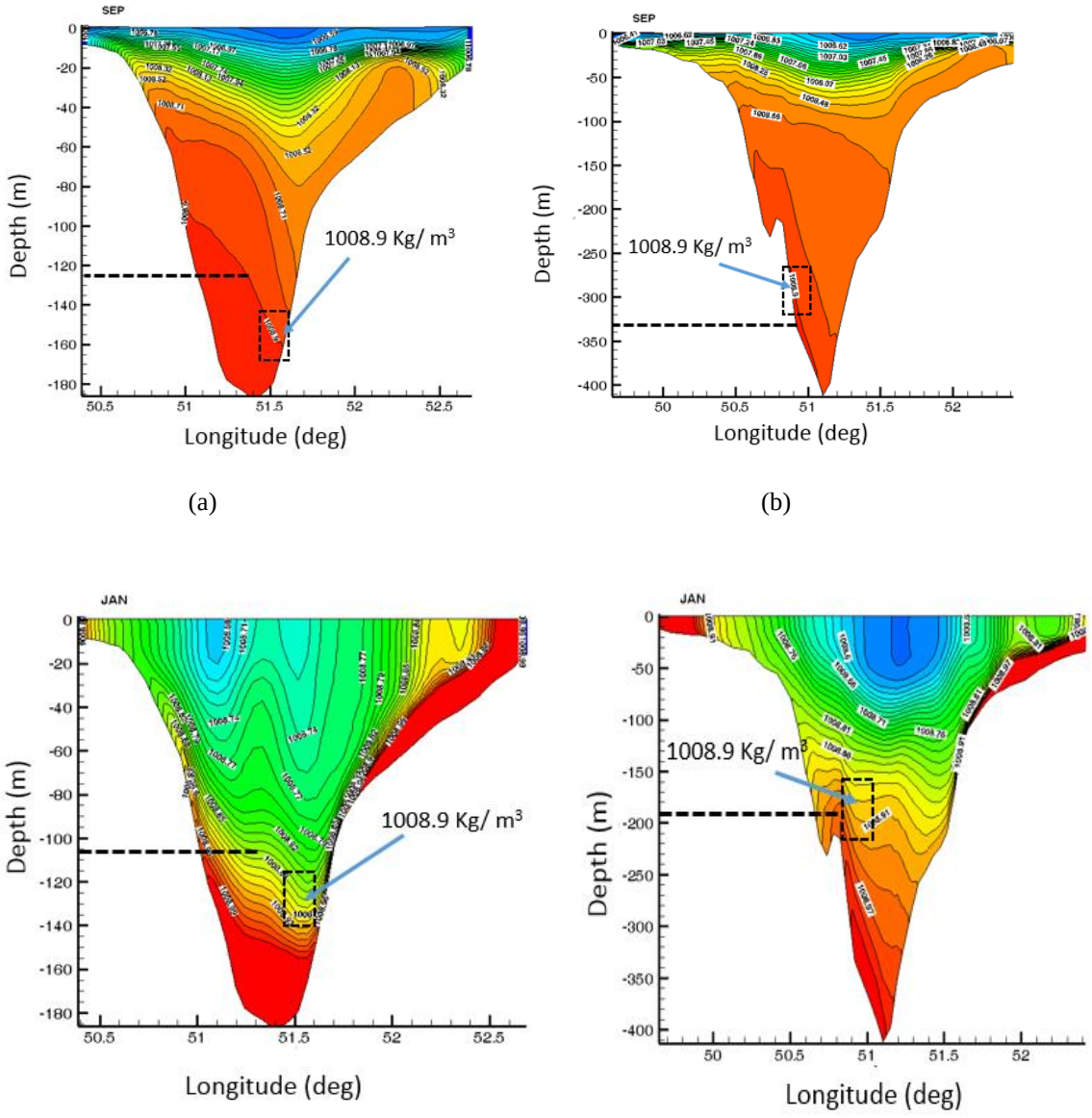

Fig 10: Simulated density fields along transects I (a) and II (b) in Sept. (above) and January (below) 2004. The reference isopycnal of the deep flow boundary is also shown.

3 Dynamics of the overflow

The dynamics of the deep flow can be analyzed using analytical models as have been used in many other works. Among them, one can refer to Girton et al. (2003); they used a stream tube framework to analyze the results of their observational data in Denmark Strait overflow. In this section, we investigate the dynamics of the overflow in the Caspian Sea. The flow, after entering in the southern basin deflects to the right and is trapped on the western boundary of southern basin topography. In the course of that, Coriolis, buoyancy, bottom frictions and entrainment are the most important forces which affect the deep flow (Fig 9b). A better approach would be to use a method which includes all forces affecting the flow dynamically. Although there are many quantities which are important in terms of the deep flow dynamics, the vorticity and potential vorticity are often used to investigate such flow behavior. Generally, the vorticity is one of the most important variables in the oceanography for understanding the main features of the water column when moving over a strait. It is also clear that some of the main features can be shown by numerical model simulation.

As mentioned in section 2, although the main aim of doing numerical simulations was to show the deep overflow in the Caspian Sea, the simulations also showed that after the deep overflow is trapped in the southern basin it seems to create eddies, particularly near of the Iranian coast. As the deep flow reaches the SefidRud Cape, it separates from that coast and forms one or two eddies. Similar flow behavior in the Persian Gulf outflow as it enters the Oman Sea has also been observed. The Persian Gulf outflow can separate from the Ras Al Hamra Cape in the Oman Sea while being attached or detached from the Cape depending on the outflow properties; its buoyancy varies with seasons (Ezam et al., 2012). In such flow, behaviour of the vorticity and potential vorticity of the flow column upstream of the Cape is linked to the separation of the flow from the Cape, as previous works (Ezam et al., 2012; Stern, 1980) have shown. Here the numerical simulations outputs are used to calculate the vorticity and potential vorticity along the deep flow. Falcini and Salusti (2015) presented a method to estimate the vorticity of the water column. This formula is very useful due to the consideration all of the forces which are important in the present overflow dynamics. Thus, this method is also used in the present work. Here, firstly the deep flow entrainment parameter and drag coefficient are calculated and then the dynamic model of the deep flow is discussed.

3.1 Estimation of drag coefficient and entrainment parameter of the deep flow

Johnson and Sanford (1992) estimated the drag coefficient, C_d=3×10^{-3} from the analysis of data from the Mediterranean outflow. Girton and Sanford (2003) used C_d=3×10^{-3} for the Denmark Strait and Cheng et al. (1999) studied the bottom roughness length and bottom shear stress in South San Francisco Bay and calculated C_d from 2×10^{-3} to 6×10^{-3}. To simplify the analysis, we define $r_b = \frac{c_d \mathrm{U}}{H}$ and $r_e = \frac{E}{H}$. In this study, we have conducted the analysis using C_d=3×10^{-3} and 5×10^{-3}. Hence, r_b =C_d U /H=0.003×0.2/50 ~ 1 ×10^{-5}s^{-1} and r_b= $C_d U/H$=0.005×0.2/50 ~ 2×10^{-5}s^{-1}. Here, r_b *is* the bottom friction parameter and U is the magnitude of the deep flow velocity where H is the thickness of overflow. E is an entrainment speed and defined as E =E^*×U, where E^* is the entrainment coefficient that depends on the overflow top boundary Richardson number (Price and Bringer, 1994).Ri is the bulk Richardson number defined as $Ri = \frac{g'H}{U^2} cos\theta$, where θ is the bottom slope. There are many

methods to calculate entrainment parameter, E^* of which some are presented in table 2. Due to the importance of E^* in the next section for estimation of vorticity, the E^* is calculated based on table 2 formulas, for the transects I, II, III, IV, and V. Figure 11 shows E^* versus Ri for May from transects I to V.

Based on Ri for the overflow, Ri varies at different locations. Using U as 0.1 to 0.2 m/s, g'=0.00222-0.00251 m/s^2, H=50-70 m, tanθ=0.02, $Ri = \frac{0.00251\times50}{0.2\times0.2}$ 0.99~ 3.1. Based on table 2 with Ri>= 0.8, we used mean E^* based on formulas 2, 3, 4 and 5 of table 1, because we cannot use the formula 1(Ri>= 0.8, then E^* <=0). For this section, r_e, entrainment parameter, values are considered as 5×10^{-6} and 1×10^{-5}s^{-1}based on typical values for Ri, U and H.

Table 2: Some of the published E^* equations based on Ri (Kashefipour et al, 2010).

Equation number	Researcher	Year	Equation
1	Ellison and Turner	1959	$E^*=\frac{0.08-0.1Ri}{1+5Ri}$
2	Ashida and Shinzi	1977	$E^*=0.0015Ri^{-1}$
3	Garcia	1985	$E^*=\frac{0.075}{(1+718Ri^{2.4})^{0.5}}$
4	Kessel and Krancnburg	1996	$E^*=\frac{5.5\times10^{-3}}{3.6Ri-1+\sqrt{(3.6Ri-1)^2+0.15}}$
5	Karamzade	2004	$E^*=0.0021\ Ri^{-1.1238}$

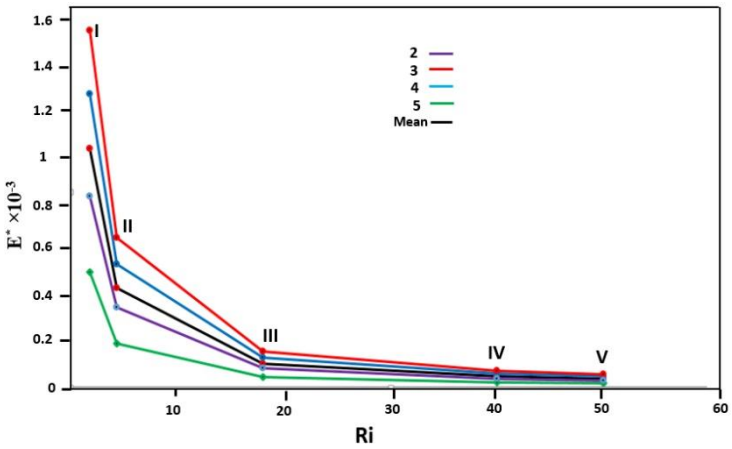

Figure 11: Changes of entrainment coefficients based on different Richardson numbers for May in transects shown in figure 1b. The formulas in table 1 are used to estimate E^* (the numbers refer to the equation numbers in table 1). To use E^* in Eqs.1 and 2 (Section 3.2), the mean values for E^* is also estimated (black).

3.2 The changes of vorticity and potential vorticity of the overflow

As mentioned before, vorticity is an important parameter for the study the column properties of overflow over the sill. Also, the vorticity can be useful to consider the behavior of the flow (e.g. Stern, 1980) in the southern basin, particularly near the SefidRud Cape. Not only do we try to estimate the vorticity of the water column and the width of the flow when moving into the southern basin, especially during the adjustment of the flow width, but also we estimate the flow vorticity and its behavior near the Cape. The width of the flow is calculated directly from the numerical simulations but for the calculations of vorticity and PV (potential vorticity), we need to use an analytical model.

Here we consider the structure of the flow as it moves over the sill in terms of its vorticity and PV. Falcini and Salusti (2015) presented an analytic model for the Sicily channel: vorticity and PV equations are based on the stream-tube model (Smith, 1975; Killworth, 1977). To deal with this, they used (ξ, ψ) coordinate system, a modified form of that which was used by Astraldi et al. (2001). In this frame, ξ is the along-flow coordinate and ψ is the cross-flow coordinate (see Figure 1 in Smith, 1975). In this method, friction and mixing effects are considered in the estimation of potential vorticity. Firstly, Falcini and Salusti used the hydrostatic pressure equations for three layers to achieve some equations for entrainment and friction; next, they concentrate on the third layer (with dense water near the bottom) to obtain formulas for vorticity and potential vorticity. In addition to this, based on their assumptions (Falcini and Salusti, 2015), the velocity of a stream line is a function of ξ only. They defined β as the angle between (ξ, ψ) and (x, y) coordinates. They assume that β is close to zero in the channel. They then used the classical vorticity equation (Gill, 1984) and assumed cross sectional averages of the various terms in the steady state of vorticity equation due to difficulty of depth and velocity calculations in different position from hydrographic data. They presented formulas (1and 2) to calculate vorticity and potential vorticity for dense flow (deepest moving layer)

. These formulas are based on a homogeneous bottom water vein while using shallow water theory (over bars indicate cross sectional averages). To obtain a formula, the bottom water is assumed to be well mixed and the flow has a strong axial velocity, nearly uniform over the cross section of the stream and also the cross-stream scale is assumed to be much smaller than the local radius of curvature of the streamline axis. Relative vorticity and potential vorticity distributions of the deep flow are:

$$\frac{\bar{\zeta}}{f} = \frac{\bar{u}_0}{\bar{u}} e^{-\int_0^{\xi} \frac{r_b}{u} dx} \left(\frac{\bar{\zeta}_0}{f} + \frac{1}{\bar{u}_0} \int_0^{\xi} e^{\int_0^{x} \frac{r_b}{u} dx'} \left[\frac{\bar{u}}{\bar{h}} \frac{\partial \bar{h}}{dx} - \frac{E}{\bar{h}} \right] dx \right. \quad \textbf{(1)}$$

$$\Pi = e^{-\int_0^{\xi} \frac{\Gamma}{u} dx} \left[\Pi_0 - \int_0^{\xi} e^{\int_0^{x} \frac{\Gamma}{u} dx'} \frac{r_b \zeta}{hu} dx \right] \quad \textbf{(2)}$$

Where $\Gamma=\frac{E}{h}$.

To obtain formula (1), it is supposed that $\overline{\zeta_0} \ll f$. After integrating the shallow-water equations along the flow and mass continuity equation and also using some mathematical operations, Eqs. 1 and 2 are obtained.

Here ζ and Π are respectively the mean relative vorticity and potential vorticity, h is the layer thickness and $\partial h/\partial x$ is slopes of the flow reference isopycnals, ζ_0 and $\overline{u_0}$ are respectively the initial vorticity and velocity. ζ_0 is estimated as U/W, where U and W are respectively the flow speed (~ 0.2 m/s) on the sill and cross channel scale (~ 20 km) over the sill. To be applicable, some terms in Eq.1 are considered as cross-sectional averages. Three terms are significant in vorticity: the stretching term, the entrainment effect and the friction. To estimate all parameters in these formulas, we use 5 transects from the Strait (I) to the southern area (V) (figure 1b). Typically, for November in transect III, $\partial h/\partial x \approx 0.0047$ ($\delta h \sim 180$ *m and* $\delta x \sim 38$ km), $\bar{u}$=0.11 m/s, $\bar{h}$=180 m, are estimated. The calculations of r_b and r_e are based on Ri number (presented in section 3.1 and formulas in table 1). Thus, $r_b=2\times10^{-5}$ (s^{-1}) and $r_e=4\times10^{-6}$ (for transect II), 8×10^{-7}(for transect III) are calculated based on (figure 11). In transect IV and V, $r_e \sim 0$ because of large Ri~ 40 to 50. Using Eqs.1 and 2, profiles of ζ and Π are plotted in figures 12 as functions of ξ along the stream tube.

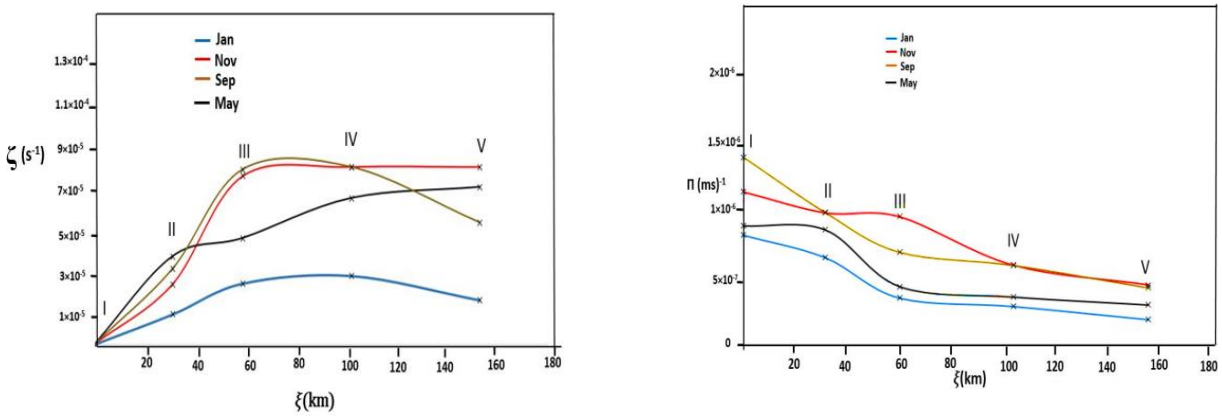

Figure 12: Changes in $\zeta(s^{-1})$ (left) and Π ($m^{-1}s^{-1}$) (right) along the flow based on Eqs. 1and 2.

Figure 12 shows that ζ increases from I to V, because of stretching term in Eq. 1, although Sep. and Jan. values have different behaviors in transect IV to V. However, after the transect III, the changes are not considered, because the depth does not vary significantly (stretching term) and entrainment has been ignored as Ri is large after this transect. In the month of November, the vorticity has a maximum value of about 8.5×10^{-5} (s^{-1}) in transect V, although in January the vorticity is the least among all the months shown. When it comes to Π, the graph shows a decrease in PV values along the flow from I to IV, but after IV, the Π values are almost constant. For example, changes of Π over the sill (from I to III) are about 7×10^{-7} ($m^{-1}s^{-1}$) and 4×10^{-7}($m^{-1}s^{-1}$) for Sep. and Jan. respectively, due to bottom friction and entrainment.

Transects I, Π and III are located on the slope and IV and V are in deeper parts of the southern basin. The vorticity and PV values are based on the topography of the Caspian Sea. Fig. 12 shows that the changes of vorticity are more marked from I to III because the depth of the flow changes more on the slope (stretching term) over this distance. As the flow enters the southern Caspian Sea basin, it adjusts into an internal Quasi-geostrophic flow, almost as a deep western boundary current in the southern Caspian Sea basin. The gravity-driven flow appears as a trapped current after Absheron sill due to Coriolis effect (transect IV and V). When moving along the southern (Iranian) coast, the forces of pressure gradient and Coriolis balance the force of friction. The entrainment effect can be ignored because the Richardson number is about 50 based on Fig. 11 in transect V, so $E^*\sim 0$. The width of flow over the sill and when being trapped is calculated for all month (from the numerical simulation results) and varies for various seasons; here it is shown for the transect V. These values are 18, 16, 34, and 35 km for Nov, Jan, May, and Sep respectively. As figure 12 shows, the potential vorticity of the water column decreases from I to V, due to frictional and entrainment effects. The comparison of the flow width from I to V transects also shows that the bottom friction (and also entrainment, particularly over the Strait) increases the width of the flow in the southern basin. For example, for September, the width of flow increases from 20 km (I) to 35 km (V), by about 15 km as a result of moving over the sill and into the southern basin. It means that friction force decreases potential vorticity of the flow in the southern basin.

Apart from this, the trapped current continues moving into the western part of the southern basin (Fig. 13), but it shows an interesting behavior as it reaches the Delta SefidRud cape. The flow separates from the cape and forms one or two eddies (Fig.14). Based on the numerical results, separation of the dense flow from the cape depends on the season (different boundary currents for different seasons). The important parameter determining the behavior of flow when it separate from the cape is its potential vorticity.

In this section, the potential vorticity of the deep flow is estimated for different seasons based on information as in figure 14. We can observe different behavior of the flow when separating from the cape for fall in November and in spring (May; Fig.14). For example, in transect V for November and May, the values of the potential vorticity are 6×10^{-7} and 4×10^{-7} $(ms)^{-1}$ respectively (Fig.12). Figure 14 indicates that in November, the flow is closer to the cape than in May during the time of separation. It can probably be concluded that the potential vorticity upstream of the flow can be effective on the flow when it separates from the cape, although other factors such as Rossby number is also important. In order to be more accurate, Stern (1980) showed that for this kind of the flow with zero potential vorticity assumption, the flow separates from the cape when the width of flow upstream of the cape is less than about 0.42 R_D, where R_D is the Rossby radius of deformation $R_D= (g´H)^{0.5}/f$ (based on the current depth, H and its reduced gravity, $g´$ far upstream). Based on Fig. 12, we can still use the Stern method for this flow, although the potential vorticity is not quite zero upstream of the Cape (figure 12, right). Based on typical values of the $R_D\sim 2L$ which is about 30 km, and width of the western boundary current (about 15 to 35 km, calculated above) which is of the same order as $0.42R_D$, the flow may just be separated from the cape especially for Jan and November (with width 16 and 18 km respectively). Fig. 14 indicates separation and formation of a cyclonic mesoscale eddy near the cape are more pronounced in November. Considering the fact that PV of the flow is not quite zero before the cape, the Stern criteria

may not apply for such flow separation. A more rigorous criterion is needed for the separation of such flow from the cape that may be dependent on the geometrical dimensions of the cape as well.

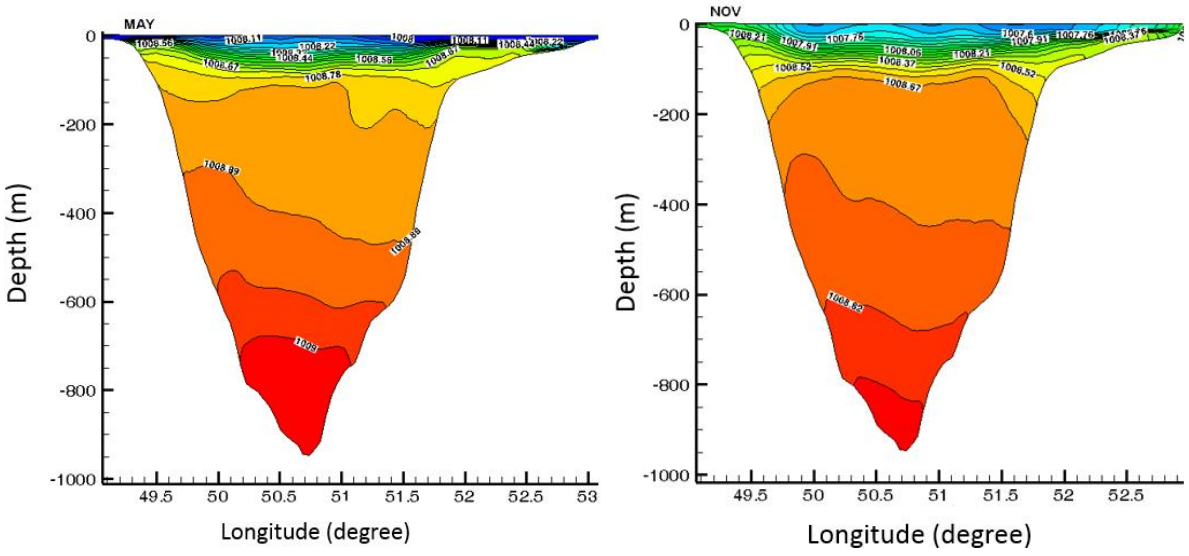

(a) (b)

Figure13: Density fields along transect V (from the numerical model) in May (a) and Nov. (b).

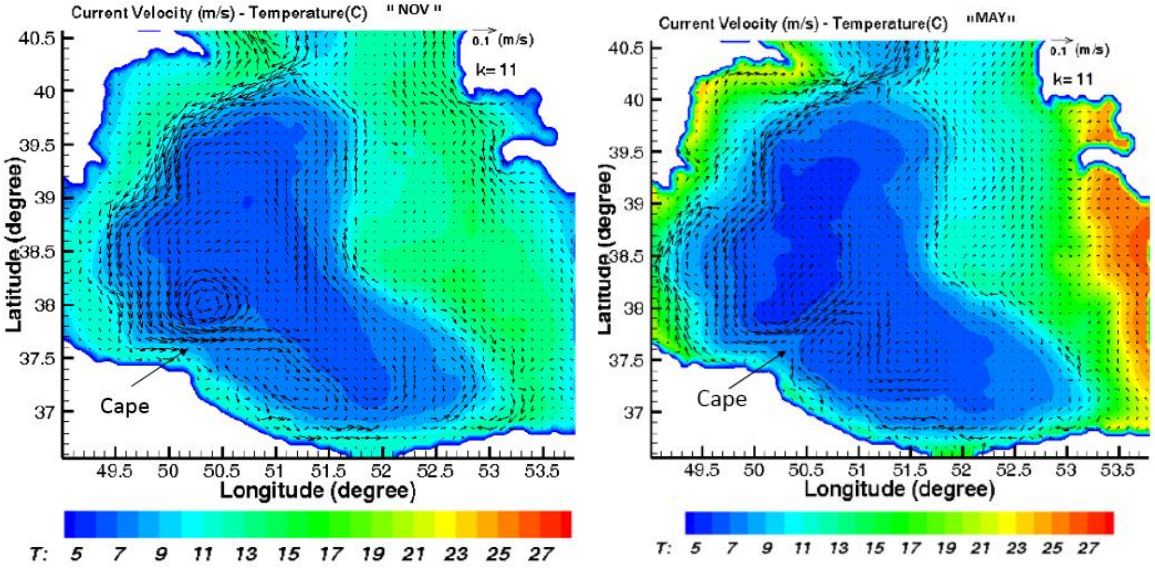

(a) **(b)**

Fig.14: Monthly mean currents (m/s) in the layer "k=11", obtained from the model simulation for May (a) and Nov (b)**.** The dense flow separates from the SefidRud Delta cape. The bottom deep topographically trapped current over the Absheron sill and the southern Caspian Sea basin is marked. k=1 is the bottom layer and k=30 is the top layer.

4. Flushing time and the importance of this work

4.1 Volumes of basins' dense water and flushing times calculations

As mentioned in section 2 and also discussed in the following section, the flushing times of the Caspian Sea basins are important parameters for this ecosystem. To calculate the basin flushing time, the first and important step is the estimation of the dense flow volume flux when entering the southern basin over the Absheron sill. A simple method to calculate the deep flow volume flux is multiplying the mean velocity of the overflow by its cross-section (Eq.3). Although the numerical model outputs give directly the velocity, the cross- section should be calculated. Here the deep flow volume flux is also estimated by formulas 3 to 6, in addition to that obtained by the numerical simulations.

It is very useful to use an equation which is compatible with the physical conditions of the Absheron sill. For this reason, the shape of the sill and the deep flow reference isopycnal will be considered for obtaining an appropriate formula (6) for the deep flow volume flux. Here the accuracy of this formula is checked using the numerical simulation results. Although use of observational data is common for deep flow volume flux estimation, we do not have ADCP data across the Absheron sill. Hence, here we try to obtain a formula using temperature and salinity data that are much more available than the ADCP data across Absheron Strait.

The overflow volume flux is given by (3) in which v is the mean magnitude of the geostrophic velocity of the overflow and ds is an element of its cross-section area.

$$Q_V = \int v\,ds \qquad \textbf{(3)}$$

Due to the parabolic form of the bottom topography (Z) of Absheron Strait, its geometry and the upper surface of the dense overflow in this valley like shape (Figure15a, b) can be given by:

$$\begin{aligned} Z &= ax^2 + bx + c \\ h' &= Ae^{-\alpha x} \end{aligned} \qquad \textbf{(4)}$$

Where a, b, c, A and α are assumed to be constant and we also assign the deep flow reference isopycnal depth (approximately the top boundary of the overflow) as h' (see Figure 15b).

Due to the fact that Z and h' (deep flow isopycnal reference line) in the graph (Figure15a, b) are from L_1 to L_2, we can calculate h' and Z values at (x=L_1) and (x=L_2), Substituting Eq. (4) in Eq. (3) and using the assumptions and that v is the mean deep flow geostrophic speed and is assumed constant (in each month and uniform in depth) and is given by the slope of h' in the x-direction, we have:

$$Q_V = \frac{g'}{f}\frac{H_1 - H_2}{|L_2| + |L_1|}\left[\left(-\frac{A}{\alpha}(e^{-\alpha L_2} - e^{\alpha L_1})\right) - \frac{a}{3}(L_2^3 + L_1^3) - \frac{b}{2}(L_2^2 - L_1^2)\right] \qquad \textbf{(5)}$$

Where:

$$a = \frac{H_2 L_1 + H_1 L_2}{L_1(L_2^2 + L_1 L_2)}$$

$$b = \frac{H_2 L_1 + H_1 L_2}{L_2^2 + L_1 L_2} - \frac{H_1}{L_1}$$

If we assume that $L = \frac{|L_1| + |L_2|}{2}$, we have

$$Q_V = \frac{g'}{f}\frac{H_1 - H_2}{|L_2| + |L_1|}\left[\frac{2A}{\alpha}\sinh(\alpha L) - \frac{2}{3}aL^3\right] \qquad \textbf{(6)}$$

Where:

$$a = \frac{H_2 + H_1}{2L^2}$$

$$b = \frac{H_2 - H_1}{2L}$$

$$A = \frac{H_1}{e^{\alpha L}}$$

$$\alpha = -\frac{1}{2L} Ln \frac{H_2}{H_1}$$

To obtain the Eq. 6, which is an approximation for $|L_1| = |L_2|$, we defined L based on L_1 and L_2. Although the minimum of Z is not exactly at x=0, it does not create a large error. To show this in reality, the Q_V is calculated separately with Eq. 5 and 6. The results show that the difference is about 2-5 percent when using (Eq. 5) without any assumptions ($L \sim |L_1| \sim |L_2|$). Another important point is that the geostrophic balance between v and h' is assumed as $R_o \sim 0.1$ based on flow parameters estimations of section 2.

To calculate the mean monthly volume flow rate of the deep current that enters the southern basin of the Caspian Sea, we assume that its density is greater than 1008.78kg/m^3. Then the average density (for different seasons) of the flow below the deep flow upper boundary (e.g. Figure15), equation (6) and figure15 are used to calculate the deep flow volume flux.

For the times that the middle and southern basins are filled, first the volumes of middle (V_M), and southern (V_S) basins (see Figure 15c) are calculated below three levels (z=0, z=-100, and z=-180 m which is the approximate depth of the Absheron sill, which would be more appropriate only for the southern basin). Then if we assume a similar annual mean value of Q_V for both

basins, these filling times are estimated. The results of these calculations and comparisons between them for different seasons are given in Tables 3 and 4. The results show that the maximum and minimum flow rates of abyssal water that enter the Southern Caspian Sea are in May and November respectively. In order to check the accuracy of Eq. 6, the Q_V is also directly calculated from the numerical simulations without any assumptions. As shown in table 3, the numerical model value is greater than that of the analytical estimation. This underestimation by Eq. 6 can be due to the fact that we used some assumptions to obtain Eq. 6. The velocity used is the geostrophic velocity and the deep flow isopycnal reference lines are also simplified. Apart from this, some errors come from the choice of 1008.78 kg/m^3 contour as its position changes for different months (see section 2.3). To solve this problem, we follow one method for all months (under the same boundary conditions for all months), to acquire approximate estimates. The flushing time is then estimated based on the direct calculation from the numerical simulations. The results show that the flushing time is about 6-7 years (middle basin) and 13-15 years (southern basin) for the numerical simulations based on z=0, that are similar to those from the Eq. 6 (table 4).

The Eq. 6 can also be useful for estimation of the volume flux of overflows in other Straits, particularly in oceanic contexts without ADCP data, for example the Persian Gulf for which there are many CTD data in the Hormuz Strait (Bidokhti and Ezam, 2009).

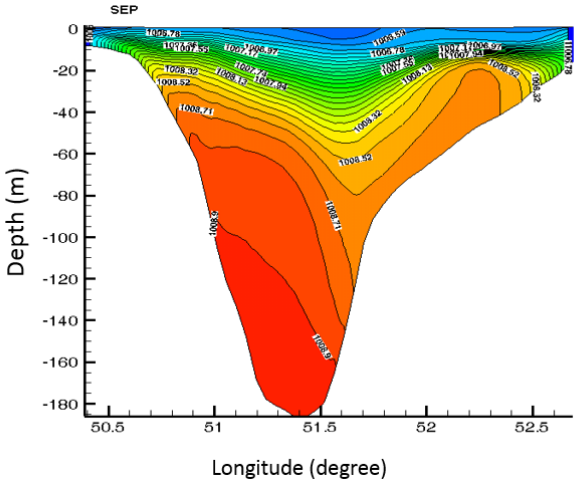

(a)

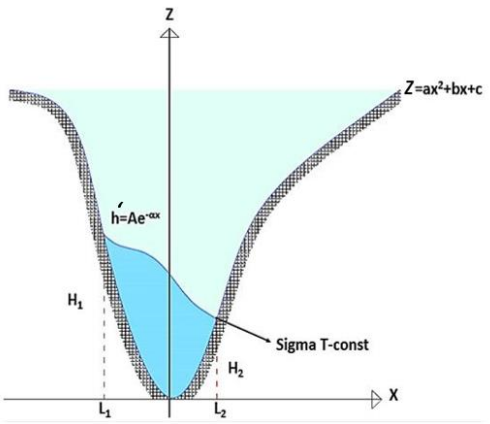

(b)

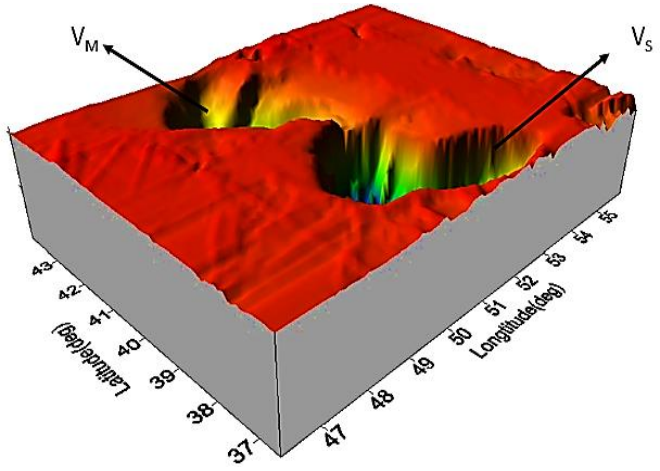

(c)

Fig15: (a) Typical density fields along transect I for Sept. from which we calculate the flow rates. (b) The scheme of the topography with a typical isopycnal and model parameters. (c) The model bathymetry used to calculate the volumes of the middle (V_M), and southern (V_S) basins. The Surfer software is used to plot and calculate V_M and V_S using GEBCO data with 0.5º × 0.5º resolution.

Table 3: The model deep flow boundary current parameters (1 *Sv*=10^6 m^3/s) for different months. The last column (red symbol) show direct calculation from the numerical model

	H_1 (m)	H_2(m)	$2L$ (m)	Q_V(Sv) Analytical	Q_V(Sv) Numerical
NOV	55	10	19000	0.016	0.034
JAN	145	85	32000	0.115	0.15
MAY	145	55	34000	0.146	0.17
SEP	135	45	27500	0.116	0.16

Table 4: Flushing times of the middle (T_M) and the southern (T_S) basins (using an annual average volume flow rate (Q_V) below three levels based on formula 6.

Level	V_M($m^3\times10^{13}$)	V_S($m^3\times10^{13}$)	T_M(year)	T_S(year)
z=0 (sea surface)	2.55	5.12	8.35	16.77
z=-100	1.09	4.13	3.57	13.5
z=-150	0.36	3.62	1.17	11.85

4.2 The importance of deep flow in the southern basin

In section 4.1, we estimate the Caspian Sea basins' flushing times because they are very important for the ventilation of these deep basins. In addition to this, in section 2, it was discussed why this time scale is important for the required time of the numerical simulations of the Caspian Sea, particularly for the deep parts proper adjustment. In this section, the importance of other aspects of the deep flow are discussed. In general, deep flows play a pivotal role in the water ventilation of deeper parts of the Caspian Sea. Signs of life in the deep part of the Caspian Sea are observed, especially in the Southern basin (Terziev, 1992), however, the reasons for the existence of marine life have not been addressed clearly so far. The main reason why the deeper part of the Sothern Caspian Sea basin is not "dead" like that in the Black Sea is that oxygen is carried from the surface layers to the bottom layers, and nutrients from the bottom layers towards the top layers by a slow advection. As a result of this, the Absheron sill overflow can be considered as the most important element of this ecosystem in the southern basin of the Caspian Sea. Moreover, these days, oil well pollution and climate change effects are the most important problems in the Caspian Sea. To begin with, it is interesting to look at the locations of the oil and gas wells in this Sea. As the location of the oil and gas wells in this basin are shown in figure 16a, it can be seen that they are mainly situated in two areas in the northern basin and particularly around Absheron sill (at present). Also, a satellite image shows that some oil spills have occurred in the vicinity of these oil and gas wells around the sill. For example, the figure16b which is extracted from Marina and Yu Lavrova (2015) using satellite data shows that the spills are located on the sill and also in the western parts of the southern basin. In addition to this, studies on the sea bed in the Absheron Strait and Bako Gulf indicated approximately 1 and 1.5 meters depth of sludge and oil residues in the form of high-density pellets and mazut (Escani and Amini, 2013). If we consider all of the points and look at the path of the deep flow (Fig.14), the present work can be very important for consideration of the impacts of such oil exploration activities in the fate of deeper as well as other depths of this environment, if certain careful actions are not taken.

By considering these points, the existence of deep flow on the sinking and mixing processes is very important in the ventilation of the southern basin. Unfortunately, the pollution of oils can spread into deeper parts of the southern basin via this deep flow. In other words, this deep flow plays a positive role in the ventilation of the deeper parts of the Caspian Sea, but with oil

exploration activities at the bottom of this enclosed sea, this deep flow can have a negative effect on the Caspian Sea, as it can carry polluted materials to the deep parts of this ecosystem.

The overflow direction was calculated showing that the flow passes over some oil drill holes on Absheron sill. Due to this angle, the flow passes over the wells near the Azerbaijani Republic rather than the eastern part of the sill near Turkmanestan. In section 3, the dynamics of the flow was discussed. Among all of the dynamics aspects, it was found that under certain conditions the flow was separated from the SefidRud Cape (based on section 3.2) and two eddies were formed here. Eddies are very significant in the ocean (Gill, 1984) because they advect mass (here the oil pollution or even harmful algae blooms) and their ability to propagate is crucial to their contribution to marine mixing (Friel, 1987). Based on the path of the deep flow and the eddy formation near SefidRud Cape, it can be concluded that the region near the SefidRud Delta Cape may be the most polluted waters in deeper parts at present and that pollution can spread other deeper parts of the southern basin of the Caspian Sea (Fig.16b).

These days, climate change leads to many problems in this area like sea level rise (Chen et al., 2017), mainly due to the rising trend of atmospheric temperature in recent years. Due to this problem, a question is raised regarding the effect of climate change on the deeper flows of the Caspian Sea. At present the water sinks in the northern basin and after filling the middle basin it finally overflows into the southern basin. If the atmospheric temperature rises, it will also warm the northern part of the Caspian Sea, and hence it is predicted that the sinking process will be weaker. As a result of this, the volume of water in the deep overflow would decrease and flushing time would increase. In other words, warming probably has a negative effect on the deep part of the southern basin of the Caspian Sea due to weaker ventilation by this deep flow, if it does not totally shut off this ventilation.

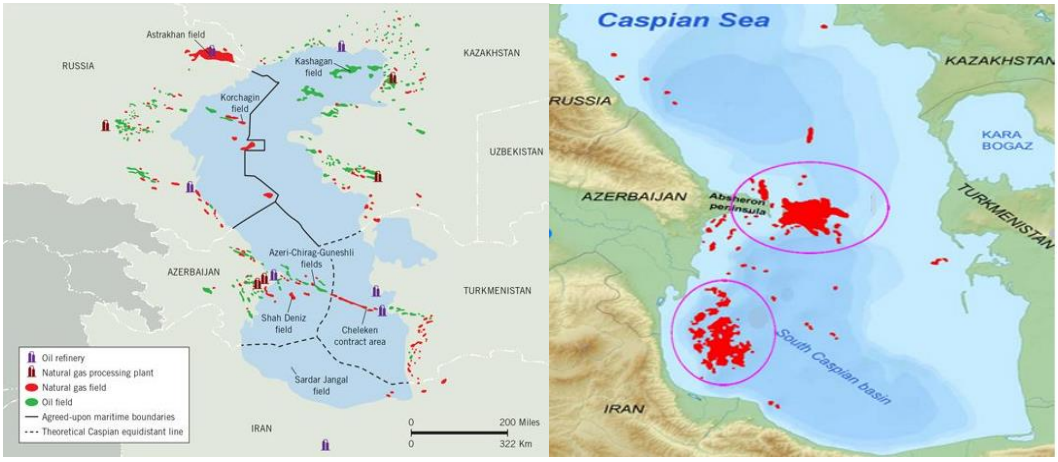

(a) **(b)**

Fig 16: (a) The locations of oil and gas fields in the Caspian Sea, extracted from *https://www.offshore-mag.com*. (b) The map of oil spills revealed from satellite radar imagery in the central and southwestern parts of the Caspian Sea in 2010. (Mityagina and Yu Lavrova, 2015).

5. Conclusions and consequences

The results of observations and numerical simulations showed that there is an abyssal flow from the middle to the southern basins of the Caspian Sea. The density difference between the deeper water of the middle basin and that of southern basin leads to an overflow gravity current over the Absheron sill. This difference is mainly due to the temperature difference between deeper parts of these two basins; winter storms and cold wind provide the cooling of this rather high-latitude shallow water in the northern basin. As a result, cold water initially sinking in the northern part of this Sea, at about 48 degrees latitude, fills first the middle basin and then overflows towards the southern basin. In autumn and winter, surface water cools and its density is increased and then it sinks to the deeper parts of the middle basin, like deep convection in high latitude oceans.

We estimated typical mass transport and flushing times of the deep-water basins of this Sea using the overflow properties at the Absheron sill. After the sill, the overflow adjusts itself moving south as a gravity-driven topographically trapped current, spiraling into deeper parts due to bottom friction and entrainment. It always tends to move toward the western shores of this Sea, mainly due to the Coriolis force that shifts it to the right. Such flow is important in the abyssal circulation and ventilation of the deep southern basin of the Caspian Sea. For vorticity and potential vorticity of the flow, the formulas which are presented by Falcini and Salusti (2015) are used to estimate the changes of relative vorticity and potential vorticity of the trapped current over Absheron sill. Results also showed that nearly 3.05×10^{12} m^3 of water per year by this abyssal flow can enter the Southern basin, giving a typical flushing time of about 15 to 20 years which is of the same order as those estimated by Peeters et al. (2000). Some points are discussed as how the southern Caspian Sea basin ecosystem can be strongly dependent on this flow.

The northern and middle Caspian Sea basins have become important areas for oil and gas explorations (especially the Absheron shallow Strait area) and marine transport nowadays. Since the Caspian Sea is an enclosed sea, the adverse effects of such activities may particularly affect the deeper parts of the Caspian Sea basins. For this reason, it is recommended that more detailed observational data are collected in the deep parts of the southern and middle basins of the Caspian Sea, by joint projects with neighboring countries. More extensive and fine-resolution observational data and numerical simulations are required to find more details of the overflow structure over and around the Absheron sill (Strait) and the deeper parts of the Caspian Sea basins.

Acknowledgments

The financial support of the University of Tehran, while doing this work is greatly acknowledged. Numerous comments of Prof.J. M. Huthnance in improving the paper is greatly acknowledged.

References

Arakawa, Akio, and Max. J. Suarez: Vertical differencing of the primitive equations in sigma coordinates, Monthly Weather Review 111.1, 34-45, 1983.

Astraldi, M., Gasparini, G. P., Gervasio, L., & E. Salusti: Dense water dynamics along the Strait of Sicily (Mediterranean Sea), Journal of Physical Oceanography 31.12, 3457-3475, 2001.

Ashida, Kazuo, and E. Shinzi: Basic study on turbidity currents, Proceedings of the Japan Society of Civil Engineers. Vol. 1975. No. 237. Japan Society of Civil Engineers, 1975.

Aubrey, D. G., Glushko T. A., and V. A. Ivanov: North Caspian Basin: Environmental status and oil and gas operational issues, Report for Mobil-oil 650, 1994.

Aubrey, D. G: Conservation of biological diversity of the Caspian Sea and its coastal zone, A proposal to the Global Environment Facility. Report to GEF, 1994.

Baringer, MO'Neil, and J. F. Price: Mixing and spreading of the Mediterranean outflow, Oceanographic Literature Review 3.45, 436-437, 1998.

Bidokhti, A. A., and M. Ezam: The structure of the Persian Gulf outflow subjected to density variations, Ocean Science 135-161, 2009.

Bondarenko, A. L: Currents of the Caspian Sea and formation of salinity of the waters of the north part of the Caspian Sea, Nauka, Moscow 6, 3019-3053, 1993.

Britter, R. E., and P. F. Linden: The motion of the front of a gravity current travelling down an incline, Journal of Fluid Mechanics 99.3, 531-543, 1980.

Chen, J. L., Pekker, T., Wilson, C. R., Tapley, B. D., Kostianoy, A. G., Cretaux, J. F., & E. S. Safarov: Long-term Caspian Sea level change. Geophysical Research Letters, 44(13), 6993-7001, 2017.

Cheng, R. T., Ling, C. H., Gartner, J. W., & P. F. Wang: Estimates of bottom roughness length and bottom shear stress in South San Francisco Bay, California, Journal of Geophysical Research: Oceans 104.C4, 7715-7728, 1999.

Dickson, R. R., Gmitrowicz, E. M., and A. J Watson: Deep-water renewal in the northern North Atlantic, Nature 344.6269 848, 1990.

Escani, H., and A, Amini: Impact of oil and gas industries on the Caspian Sea ecosystem. The growth of Geography Education, number 103, page 26-31, 2013.

Ellison, T. H., and J. S Turner: Turbulent entrainment in stratified flows, Journal of Fluid Mechanics 6.3, 423-448, 1959.
Ezam, M., Bidokhti, A. A., & A. H Javid: Numerical simulations of spreading of the Persian Gulf outflow into the Oman Sea. Ocean Science, 6(4), 887-900, 2010.

Falcini, F., and E. Salusti: Friction and mixing effects on potential vorticity for bottom current crossing a marine strait: an application to the Sicily Channel (central Mediterranean Sea), Ocean Science 11.3, 391-403, 2015.

Fogelqvist, E., Blindheim, J., Tanhua, T., Østerhus, S., Buch, E., & F. Rey: Greenland–Scotland overflow studied by hydro-chemical multivariate analysis, Deep Sea Research Part I: Oceanographic Research Papers 50.1, 73-102, 2003.

Flierl, G. R.: Isolated eddy models in geophysics. Annual Review of Fluid Mechanics, 19(1), 493-530, 1987.

García, Marcelo H: Hydraulic jumps in sediment-driven bottom currents, Journal of Hydraulic Engineering 119.10, 1094-1117, 1993.

Ghaffari, P., and V. Chegini: Acoustic Doppler Current Profiler observations in the southern Caspian Sea: shelf currents and flow field off Feridoonkenar Bay, Iran, Ocean Science 6.3, 737-748, 2010.
Ghaffari, P., Isachsen, P. E., and J. H. LaCasce: Topographic effects on current variability in the Caspian Sea, Journal of Geophysical Research: Oceans 118.12, 7107-7116, 2013.

Gill, A. E: Atmosphere-ocean dynamics, Elsevier, 1984.

Girton, James B., and T. B. Sanford: Descent and modification of the overflow plume in the Denmark Strait, Journal of Physical Oceanography 33.7, 1351-1364, 2003.

Griffiths, R. W: Gravity currents in rotating systems, Annual Review of Fluid Mechanics 18.1, 59-89, 1986.

Gunduz, M., and E. Özsoy: Modelling seasonal circulation and thermohaline structure of the Caspian Sea, Ocean Science 10.3, 459-471, 2014.

Huthnance, John M: Circulation, exchange, and water masses at the ocean margin: the role of physical processes at the shelf edge, Progress in Oceanography 35.4, 353-431, 1995.

Ibrayev, R. A., Özsoy, E., Schrum, C. & H. I. Sur: Seasonal variability of the Caspian Sea three-dimensional circulation, sea level and air-sea interaction, Ocean Science 6.1, 2010.

Ismailova, B. B: Geoinformation modeling of wind-induced surges on the northern–eastern Caspian Sea, Mathematics and Computers in Simulation 67.4-5, 371-377, 2004.

Johnson, G.C. and T.B. Sanford: Bottom and interfacial stresses on the Mediterranean outflow, Tenth Symposium on Turbulence and Diffusion. Portland, Oregon. American Meteorological Society, 105-106, 1992.

Kara, A. B., Wallcraft, A. J., Metzger, E. J., & M. Gunduz: Impacts of freshwater on the seasonal variations of surface salinity and circulation in the Caspian Sea, Continental Shelf Research 30.10, 1211-1225, 2010.

Karamzadeh, N: Experimental investigation of water entrainment into a density current,M. Sc. Thesis, ShahidChamran University, Ahvaz, Iran , 2004.

Kashefipour, S., Kooti, F., and M. Ghomeshi: Effect of reservoir bed slope and density current discharge on water entrainment, Environmental Hydraulics, Two Volume Set: Proceedings of the 6th International Symposium on Environmental Hydraulics, Athens, Greece, 23-25 June 2010. CRC Press, 2010.

Kessel, Thijs van, and C. Kranenburg: Gravity current of fluid mud on sloping bed, Journal of Hydraulic Engineering 122.12, 710-717, 1996.

Killworth, Peter D: Mixing of the Weddell Sea continental slope, Deep Sea Research 24.5, 427-448, 1977.

Luyten, P.J., Jones, J.E., Proctor, R., Tabor, A., Tett, P. & K. Wild-Allen: COHERENS- A coupled hydrodynamical-ecological model for regional and shelf seas: user documentation, MUMM Rep, Management Unit of the Mathematical Models of the North Sea, 1999.

Mazaheri, S., Kamranzad, B., and F.Hajivalie: Modification of 32 years ECMWF wind field using QuikSCAT data for wave hindcasting in Iranian Seas, Journal of Coastal Research 65.sp1 344-349, 2013.

Mityagina, Marina I., and Olga Yu Lavrova. : Multi-sensor satellite survey of surface oil pollution in the Caspian Sea." Remote Sensing of the Ocean, Sea Ice, Coastal Waters, and Large Water Regions 2015. Vol. 9638. International Society for Optics and Photonics, 2015.

Peeters, F., Kipfer, R., Achermann, D., Hofer, M., Aeschbach-Hertig, W., Beyerle, U., &K.Fröhlich: Analysis of deep-water exchange in the Caspian Sea based on environmental tracers, Deep Sea Research Part I*:* Oceanographic Research Papers 47.4 621-654, 2000.

Price, J. F. &Baringer, M. O. N. (1994). Outflows and deep water production by marginal seas. Progress in Oceanography, 33(3), 161-200.

Shiea, M., Chegini, V. & A. A. Bidokhti: Impact of wind and thermal forcing on the seasonal variation of three-dimensional circulation in the Caspian Sea, IJMS, Vol. 45 (05), 671-686, 2016.

Smith, Peter C: A streamtube model for bottom boundary currents in the ocean, Deep sea research and oceanographic abstracts. Vol. 22. No. 12. Elsevier, 1975.

Stern, Melvin E: Geostrophic fronts, bores, breaking and blocking waves, Journal of Fluid Mechanics 99.4, 687-703, 1980.

Terziev, F. S., Kosarev A., and A. A. Kerimov: The Seas of the USSR. Hydrometeorology and Hydrochemistry of the Seas,*The Barents Sea* 1, 1992.